A Journal of the Gesellschaft Deutscher Chemiker

Angewandte International Edition GDCh Chemie

www.angewandte.org

Accepted Article

Title: Self-assembled Helical Arrays for Stabilizing the Triplet State

Authors: Aakash D. Nidhankar, Goudappagouda - -, Divya S. Mohana Kumari, Shailendra Kumar Chaubey, Rashmi Nayak, Rajesh G. Gonnade, G. V. Pavan Kumar, Retheesh Krishnan, and Santhosh Babu Sukumaran

To be cited as: *Angew. Chem. Int. Ed.* 10.1002/anie.202005105

Link to VoR: https://doi.org/10.1002/anie.202005105

WILEY-VCH

RESEARCH ARTICLE WILEY-VCH

Self-assembled Helical Arrays for Stabilizing the Triplet State

Aakash D. Nidhankar,[a,b] Goudappagouda,[a,b] Divya S. Mohana Kumari,[d] Shailendra Kumar Chaubey,[e] Rashmi Nayak,[a] Rajesh G. Gonnade,[b,c] G. V. Pavan Kumar,[e] Retheesh Krishnan,[d] Sukumaran Santhosh Babu*[a,b]

[a] Organic Chemistry Division, National Chemical Laboratory (CSIR-NCL), Dr. Homi Bhabha Road, Pune-411 008, India.
[b] Academy of Scientific and Innovative Research (AcSIR), Ghaziabad-201 002, India.
[c] Center for Materials Characterization (CMC), National Chemical Laboratory (CSIR-NCL), Dr. Homi Bhabha Road, Pune-411 008, India.
[d] Department of Chemistry, Government College for Women, Thiruvananthapuram-695 014, Kerala, India.
[e] Department of Physics, Indian Institute of Science Education and Research, Pune-411 008, Maharashtra, India.

Abstract: Room-temperature phosphorescence of metal and heavy atom-free organic molecules has emerged as an area of great potential in the recent past. A rational design played a critical role in controlling the molecular ordering to impart efficient intersystem crossing and stabilize the triplet state to achieve room-temperature ultralong phosphorescence. However, in most of the cases, the strategies followed to strengthen phosphorescence efficiency have resulted in a reduced lifetime, and the available nearly degenerate singlet-triplet energy levels impart a natural competition between delayed fluorescence and phosphorescence, with former one having the advantage. Here, an organic helical assembly supports it towards phosphorescence in this competitive pathway to exhibit an ultralong phosphorescence lifetime. In contrary to other molecules, 3,6-phenylmethanone functionalized 9-hexylcarbazole exhibits a remarkable improvement in phosphorescence lifetime (> 4.1 sec) and quantum yield (11 %) due to an efficient molecular packing in the crystal state. A right-handed helical molecular array act as a trap and exhibits triplet exciton migration to support the exceptionally longer phosphorescence lifetime. The present work will urge new molecular designs to achieve ultralong organic phosphorescence under ambient conditions.

Introduction

Room-temperature phosphorescence (RTP) of organic molecules has been enthusiastically investigated recently for various applications such as electroluminescence, sensing, bio-imaging etc.[1,2] It has been demonstrated that the incorporation of heavy atoms and functional moieties equipped with lone pair of electrons facilitate intersystem crossing (ISC) rate (k_{ST}) through strong spin-orbit coupling (SOC), leading to efficient RTP.[3-6] In this direction, diverse molecular designs have been explored for ultralong organic phosphorescence (UOP).[7-10] Hence, successful strategies such as molecular units with n orbitals, which can reduce the singlet-triplet (S-T) splitting energy (ΔE_{ST}) and stabilize the triplet excited state through various interactions, have been widely employed.[5f] Significant advancement has been noticed in the area of UOP materials and the maximum lifetime reported for crystalline small molecule-based organic phosphor is ~2.5 s (Figure 1a, Table S1).[11] Mostly, longer lifetimes under ambient condition is achieved by stabilization of the triplet state through H-aggregation (Figure 1b). However, the already established strategies to improve the phosphorescence efficiency often lead to shortening the lifetime. Moreover, the molecular designs to enhance the nearly degenerate triplet manifolds can, in turn, facilitate reverse intersystem crossing (RISC) to exhibit delayed fluorescence (DF).[12] Hence it demands a new alternate plan of action to control the competitive decay pathways and efficiently manage the triplet excitons to enhance phosphorescence lifetime. It can be achieved only through unexplored molecular designs and with the rigorous assistance of molecular packing. As known, helical arrays of organic small molecules and polymers exhibit exciting optoelectronic properties by controlling the spatial organization of the structural units.[13] Hence, the design of a helical assembly to modulate the triplet state to achieve a longer phosphorescence lifetime will be highly appreciated. Our continuous attempts in this direction enabled us to successfully utilize the crystalline helical arrays of phenylmethanone functionalized alkylated carbazole to achieve a longer lifetime of above 4 s (Figure 1b).

Results and Discussion

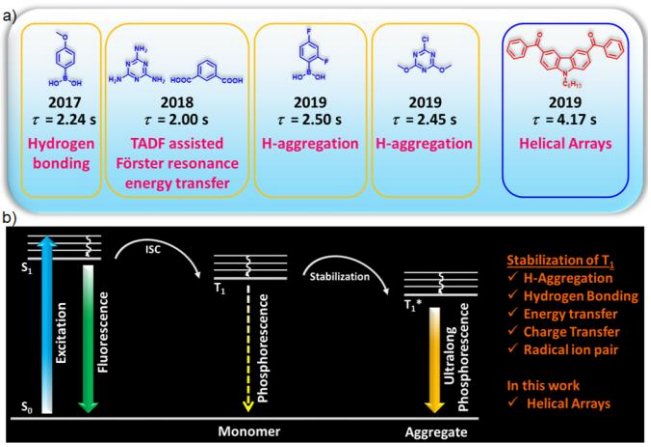

Figure 1. (a) Recent developments in the area of small molecule-based organic phosphors with lifetime above 2 s and the present work with above 4.17 s. (b) Schematic of the stabilization of the triplet state, leading to ultralong phosphorescence.

Among the potential RTP candidates, carbazole has undergone diverse functionalization using various combinations of heavy atoms and other functional groups to achieve UOP (Table S2).[8c,9b,10d,10e] We planned to study the effect of phenylmethanone functionalization on the RTP features of 9-hexylcarbazole, which exhibits very low RTP lifetime.[14] Our design strategy comprised of, i. N-alkylation of carbazole to enhance the solubility and impart alkyl-π interaction to promote

crystallization, ii. phenylmethanone unit to support a (strain-induced) crystalline assembly formation and stabilize the triplet state by providing hybrid (n,π*) and (π,π*) configurations for UOP.[15] Accordingly, a series of 9-hexylcarbazole molecules with phenylmethanone units at 3 and 3,6-positions were synthesized and unambiguously characterized by ^{1}H and ^{13}C nuclear magnetic resonance spectroscopies and high-resolution mass spectrometry (Figure 2a, Scheme 1). While our study was progressing, Chen et al., reported the effect of impurity on the afterglow property of carbazoles.[16] In the purview of this report, we synthesized carbazole in our lab using reported protocols[17] and confirmed the purity by high-performance liquid chromatography (HPLC) using acetonitrile-water mixture (Scheme 1). All the final molecules were also purified similarly and hence, we would like to mention that the concerns related to the effect of impurity on the present work, if any, are not valid.

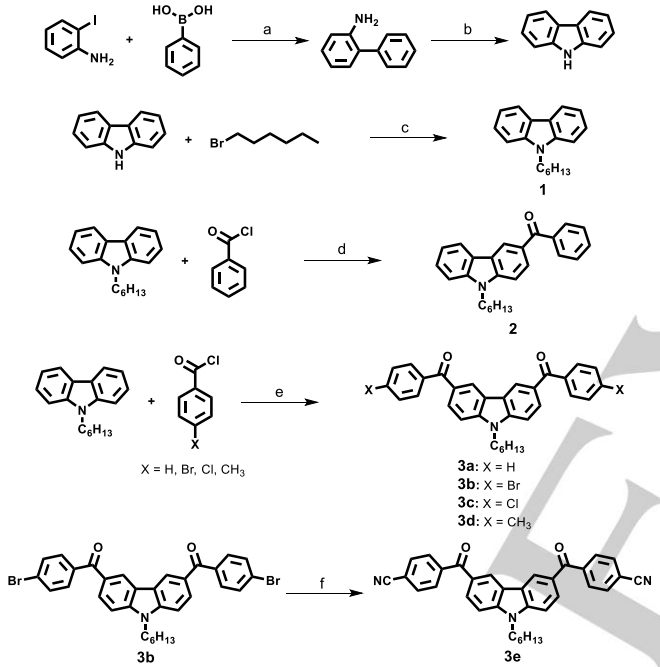

Scheme 1. Synthetic scheme for carbazole and target molecules **1**-**3e**, a) $Pd(PPh_3)_4$, K_3PO_4, EtOH, 90 °C, 12 h, 91%, b) $Pd(OAc)_2$, Imes HCl, H_2O_2 (35%), AcOH, 120 °C, 20 min, MW, 80%, c) TBAB, KOH, DMF, 70 °C, 24 h, 89%, d) anhy. $AlCl_3$ (1 eq.), anhy. CH_2Cl_2, 0 °C - 30 min, 30 °C - 12 h, 62%, e) anhy. $AlCl_3$ (2.5 eq.), anhy. CH_2Cl_2, 0 °C - 30 min, 30 °C - 12 h, 70-75%, f) $Pd(PPh_3)_4$, $Zn(CN)_2$, DMF, 110 °C, 24 h, 61%.

After the complete characterization of the molecules, we checked the thermal stability and followed by optical properties. Thermogravimetric analysis indicated the enhanced stability upon moving from molecule **1** to **3b**, indicating the importance of substitution on 9-hexylcarbazole (Figure S2). We observed a similar trend in the melting point of **1**-**3b** in differential scanning calorimetry experiments as well (Figure S3). While absorption features of all the luminogens **1**-**3b** in 2-methyltetrahydrofuran (MTHF) have not varied significantly (Figure S4), compared to **1**, the fluorescence spectra of **2**-**3b** showed a bathochromic shift of 50 nm due to the increasing electron-withdrawing ability of the carbonyl groups (Figure 2b and Table S3). An increase in the number of benzoyl groups did not alter the fluorescence maximum of **2**-**3b** in MTHF. Fluorescence lifetime decay profiles in MTHF show that the higher lifetime component varied as 4.11 ns (**1**), 6.39 ns (**2**), 6.04 ns (**3**) and 6.38 ns (**4**) (Figure S5, Table 1 and Table S4). Both red-shifted fluorescence maximum and enhanced fluorescence lifetime for molecules **2**-**3b** points to the effect of benzoylation on carbazole. A comparison of the fluorescence spectra of the MTHF solution at RT (298 K) and 77 K indicates that **1** exhibits additional long-wavelength peaks (400-550 nm) along with fluorescence peak at 370 nm, whereas a completely red-shifted fluorescence peak appeared for molecules **2**-**3b** (Figure S6, Table 1). The fluorescence spectra of **2**-**3b** both at RT and 77 K match with the red-shifted peak of **1** between 400-550 nm at 77 K (Figure S6).

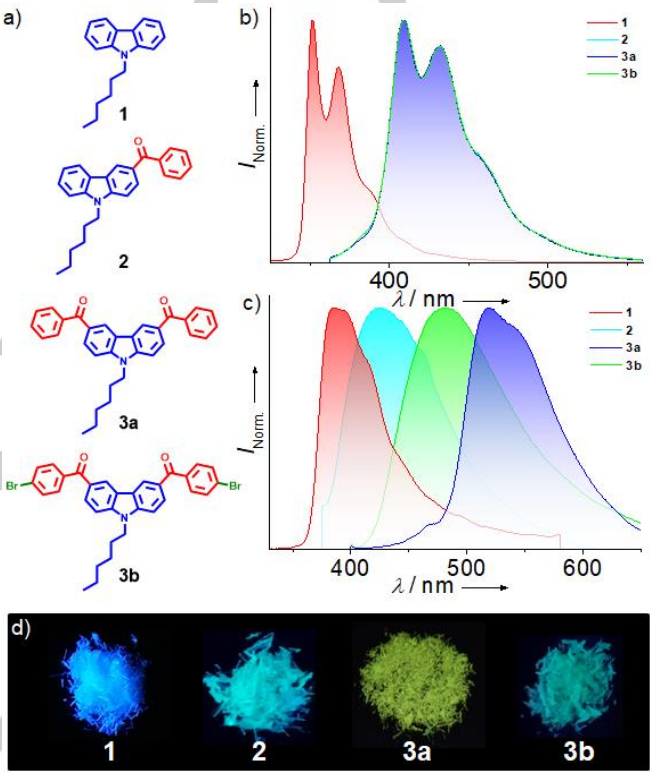

Figure 2. (a) Chemical structure of **1**-**3b**. Normalized steady-state fluorescence spectra of **1**-**3b** in (b) MTHF solution and (c) crystals at RT. (d) Photographs of **1**-**3b** crystals under UV light (365 nm).

To study further, all molecules were crystallized from CH_2Cl_2 and the morphology was visualized by fluorescence microscopy (FM) (Figure S7), scanning and transmission electron microscopy (SEM and TEM) images (Figure S8). It was found that molecule **1**-**3a** formed crystalline rods, whereas flat sheets were formed by **3b** (Figure S7,8). The bulk purity and ordering of the molecules were confirmed by matching the experimental and theoretical powder X-ray diffraction patterns (Figure S9). The diffuse reflectance spectra of crystals of **1**-**3b** exhibited a broad band between 300-450 nm, having an additional absorption band located around 360-380 nm (Figure S10). It is clear from the fluorescence spectra of crystals at RT that molecule **3a** exhibits a far red-shifted peak (λ_{max} = 517 nm) than that of **1** (λ_{max} = 390 nm), **2** and **3b** (λ_{max} = 425 and 490 nm) (Figure 2c,d). Similarly, compared to **1**, molecules **2**-**3b** exhibited a marked difference in fluorescence features at 77 K in the crystalline state (Figure S11). The presence of a long-lived component in the

fluorescence lifetime decay of **2**-**3b** was noticed when the lifetime was monitored at the fluorescence maxima. Hence, to find out the fluorescence lifetime, the measurement was carried out by monitoring at lower wavelengths and the longer lifetime component varied as 11.1 ns (87%) for **1**, 1.88 ns (17%) for **2**, 3.37 ns (59%) for **3a**, and 3.23 ns (75%) for **3b** (Figure S12 and Table S4).

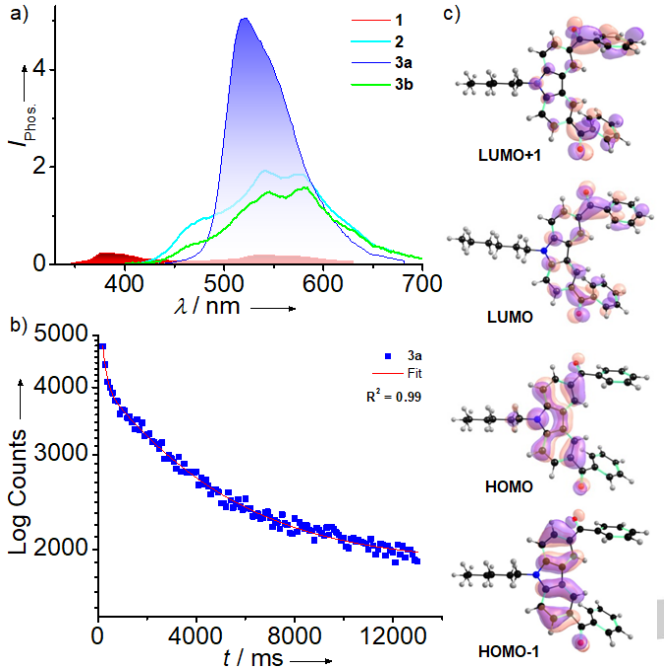

Figure 3. (a) Phosphorescence spectra of **1-3b** crystals at RT in air. (b) Phosphorescence lifetime decay profile of **3a** crystal recorded at RT in air. (c) The frontier molecular orbitals of **3a** from DFT calculations.

The red-shifted fluorescence of the crystals of **2**-**3b** at RT nearly matches with the corresponding spectra at 77 K, implying RTP for **2**-**3b** in the crystalline assembly (Figure S11, S13-16). To clarify the presence of RTP for crystals of **2**-**3b**, phosphorescence spectra were measured and confirmed that the observed red-shifted peak at RT is due to phosphorescence (Figure 3a). In the crystalline state, the phosphorescence intensity of **3a** was found to be highest among all, and it was ~27 times higher than that of **1**. The enhanced RTP for **3a** was visualized by phosphorescence lifetime measurement and it varied as 5.1, 16.6, 4171 and 114.5 ms for **1-3b**, respectively (Figure 3b, S17 and Table S5). Molecule **3a** exhibited a longer phosphorescence lifetime with afterglow for > 12 s upon excitation after just dipping in liquid nitrogen (Figure S15). The phosphorescence quantum yield of the crystals varied as **1** (3.36 %), **2** (0.85 %), **3a** (11.25 %) and **3b** (5.15 %) (Table S6,7). The observed enhancement in the phosphorescence lifetime of **3a** raised curiosity about the excited triplet state of this particular molecule, and hence we decided to study it in detail.

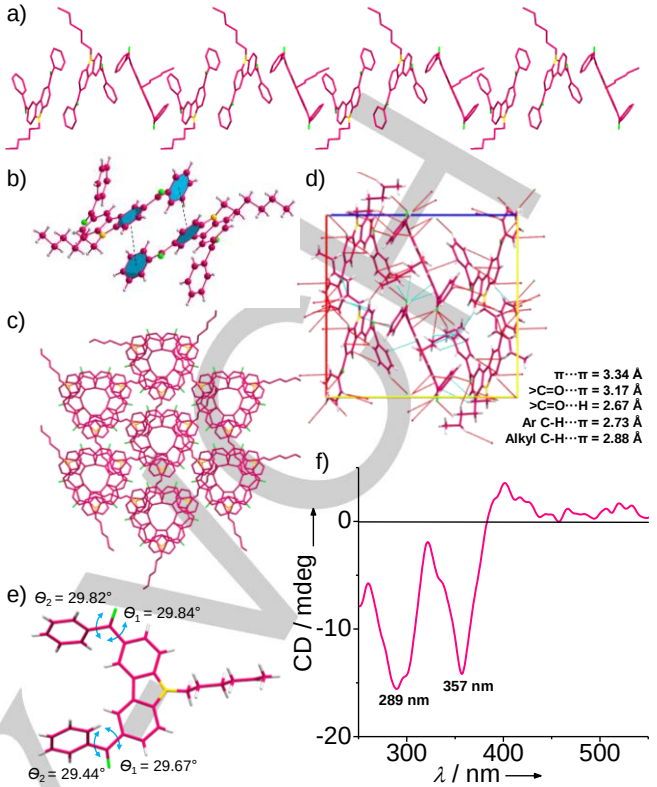

Figure 4. (a) The extended molecular packing of **3a** forming the helical 1D-array in the b-axis with the help of (b) π-π interaction between carbazole and phenylmethanone unit of the adjacent molecule. (c) Six adjacent helical arrays of **3a** leading to extended columnar packing in the c-axis. (d) All possible intermolecular interactions in a unit cell of **3a**. (e) Crystal structure of **3a** showing the dihedral angles. (f) The solid-state CD spectrum of **3a** crystals at RT.

Time-dependent density functional theory (TD-DFT) computations at the B3LYP/6-31G(d) level of theory for single-molecule in vacuum show that the electron density of the HOMO is located on the carbazole moiety and the LUMO is delocalized over the entire molecule with a considerable extension to the phenylmethanone group (Figure 3c, S18-21 and Table S6-9). The low-lying excited electronic states mainly result from well-described π-π* transitions along with a significant contribution from the n-π* character. On examining the relative computed energies for the singlet (S_n) and triplet (T_n) states for **3a**, it has been found that there are many triplet states (T_4-T_9) nearly degenerate with the first singlet excited state (S_1) (Figure S20 and Table S8). As the phenylmethanone functionalization increases, an intense mixing of nearly degenerate excited singlet and triplet states were observed, which could bring out a natural competition between ISC and RISC (Figure S20). The energetic proximity of the singlet and the triplet manifold potentials established a small ΔE_{ST}. Thus it appears that molecules **2**-**3b** have energetically well-matched states that enable efficient singlet-triplet or triplet-singlet crossings. Once T_4-T_9 levels are populated, relaxation through the triplet manifold to the T_1 state leads to phosphorescence (Figure S18-21). Besides, we have to consider the strong possibility of RISC in a competitive pathway to exhibit DF. The ΔE_{S1T1} value calculated for the monomer from DFT and phosphorescence spectra were varied as 0.72 and 0.32 eV, respectively (Figure 3a, S20, and

Table S8). It shows that the aggregation of **3a** with the assistance of intermolecular interactions reduces ΔE_{S1T1} to facilitate both ISC and RISC.

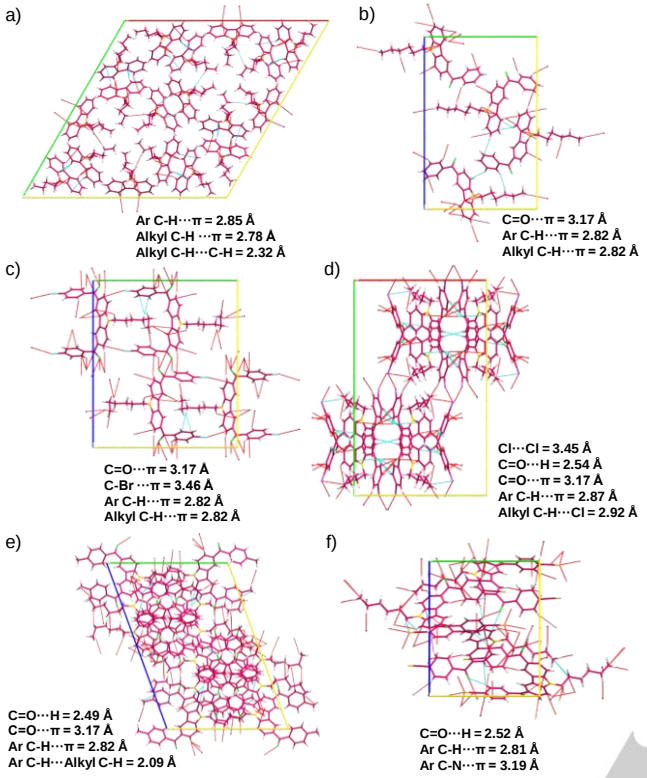

Figure 5. The molecular packing of (a) **1** (b) **2** (c) **3b** (d) **3c** (e) **3d** and (f) **3e** in the unit cell.

Single-crystal X-ray analysis has been employed to get a deeper structure-property correlation of **1**-**3b**. (Figure 4 and S22-27). The unit cell of **3a** contains six molecules arranged in a helical way in two rows along b axis using various intermolecular interactions. An extended molecular array was formed by the arrangement of molecules (Figure 4a) mainly through π-π interaction (3.34 Å) between carbazole and phenylmethanone units of adjacent molecules (Figure 4b) along b-axis. This one-dimensional (1D) helical array is stabilized with the help of CH···π interaction (2.88 Å) between the alkyl chain on carbazole and phenylmethanone unit in the adjacent helical columns to form a three-dimensional network structure (Figure 4c). We strongly believe that this kind of space filled packing (Figure 4c,d) rigidifies the molecular conformations and remarkably block the nonradiative decay pathways. The dihedral angle between the aryl groups and carbonyl subunits was found to be around 30° and it enables efficient electronic communication between carbazole and phenylmethanone *via* conjugation (Figure 4e). It can be anticipated that better communication between the (n,π*) from the >C=O and (π,π*) of carbazole could result in hybrid triplet states. The helical array of **3a** was confirmed by the solid-state circular dichroism (CD) spectrum (Figure 4f). A bisignated CD signal observed points to the right-handed helical array of molecules (Figure 4a,f). However, no such helical array is present in the case of **1**, **2** and **3b**, and mostly, a loosely packed crystalline assembly was observed (Figure 5, S21-23). Especially, **3b** packs in a kind of slipped molecular arrangement with a carbazole-carbazole distance of 5.7 Å (Figure S24). Hence, the helical array of **3a** is responsible for the enhanced RTP through an efficient space filled molecular packing by making use of maximum intermolecular interactions (Figure 4a-c).

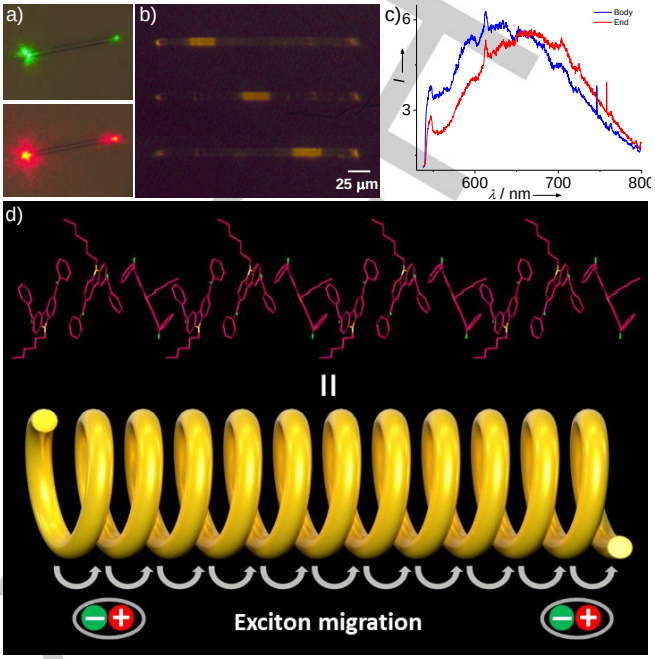

Figure 6. (a) Passive waveguiding properties of the crystal of **3a** upon excitation at 532 (above) and 633 nm (below) wavelength, the colors green and red are attributed to the excitation sources, respectively. (b) Phosphorescence waveguiding by the single crystalline rods of **3a** after filtering out the excitation wavelength (532 nm). (c) The red-shifted phosphorescence observed at the distal end of the crystal compared to the body (λ_{ex} = 532 nm). (d) Schematic of the helical array of **3a** leading to triplet exciton migration.

Recently, helical/twisted aromatic systems have been of interest to promote intersystem crossing.[18] Hence, the stabilization of the triplet state of **3a** is strongly supported by the presence of strained helical arrays. To ascertain the impact of helical arrays on such a longer phosphorescence lifetime, we prepared a series of carbazole molecules by varying the functional moieties on the phenylmethanone unit (**3c-e**) (Scheme S1 and Figures S25-37). However, molecules **3c**-**e** packed differently (Figures 5, S25-27 and Table S5, S10-12) and hence exhibited lower phosphorescence lifetimes (Figure S34 and Table S5). It indicates the critical supportive role of helical arrays to impart a longer lifetime for **3a**. Besides, we have tested the emission of **3a** in poly(methyl methacrylate) (PMMA) matrix and found that the spectral feature has been significantly changed and the lifetime also drastically decreased (8.15 ms) due to the lack of specific molecular ordering (Figure S38).

A perfectly aligned and densely packed fluorescent pi-conjugated molecular array with a large Stokes shift is known for optical waveguiding (WG).[2a,19] Hence, to check the possibility of WG, one end of the crystals of **3a** was excited at 532 and 633 nm using a 10X, 0.3 NA objective lens[20] and found that the micro rods exhibit intense green and red emissions at the distal end, respectively, with characteristic features of the optical WG (Figure 6a). The maximum phosphorescence intensity at the distal end was observed when it is excited with polarization

along the long axis of the rod, and it has been significantly reduced in the perpendicular polarization (Figure S39). Since molecule **3a** is RTP active, it is obvious that phosphorescence of **3a** propagates along the long axis of the single crystal rods (Figure 6b). The self-waveguided phosphorescence was imaged on a rod with an excitation spot (λ = 532 nm) positioned at different distances from the end of the rod (Figure 6b). To examine the secondary emission we filtered out the excitation wavelength using an edge filter. The propagation loss coefficient calculated for phosphorescence of **3a** by measuring the intensity at the distal end and the distance from the excitation point is approximately 0.028 dB/μm (Figure S40). In order to distinguish between the optical WG and exciton migration, we checked the difference in emission from the body and tip of the rods. A red-shifted phosphorescence at the distal end of the crystal compared to the body at RT was observed (Figure 6c).[21] The red-shifted emission is due to the triplet exciton migration[21,22] from the body to the tip of **3a** single crystal rods and thereby actively supports the long-lived phosphorescence (Figure 6d). In the case of other molecules, only waveguiding and no exciton migration was observed, and it points to the critical supportive role of molecular packing assisted exciton migration in achieving longer phosphorescence lifetime.

Table 1. Photophysical parameters of compounds **1**-**3e** based on fluorescence and phosphorescence experiments in the crystal state.

No	QY_{Fl} (%)	τ_{Fl} (ns)	$k_{nr,\,Fl}\,10^9\,S^{-1}$	$k_{r,Fl}10^9\,S^{-1}$	$k_{isc}\,10^7\,S^{-1}$	QY_{Phos} (%)	τ_{Phos} (ms)	$k_{nr,\,Phos}\,S^{-1}$	$k_{r,\,Phos}\,S^{-1}$
1	59.00	11.09	0.033	0.053	0.302	3.36	5.1	189.4	6.58
2	03.68	1.36	0.701	0.027	0.625	0.85	16.6	59.72	0.51
3a	13.58	2.92	0.257	0.046	3.85	11.25	4171	0.212	0.026
3b	27.14	2.53	0.267	0.107	2.03	5.15	114.5	8.28	0.44
3c	4.14	1.06	0.879	0.039	2.46	2.61	45.3	21.49	0.57
3d	4.52	6.23	0.148	0.007	0.431	2.69	6.59	147.6	4.08
3e	4.47	1.11	0.842	0.040	1.81	2.01	11.9	82.34	1.68

TD-DFT studies revealed a qualitative picture of the equal possibility of ISC and RISC for **3a** due to the presence of energetically matching sing let and triplet levels. Even though a shorter component is noticed, the unambiguously confirmed long-lived phosphorescence decay supersedes it with the support of triplet exciton migration through helical molecular arrays. The afterglow observed for more than 12 s after just dipping in liquid nitrogen supports the suppression of RISC and thereby endorses improved radiative decay through the triplet manifolds at low temperature. The efficient molecular ordering in the helical array of **3a** ensures that the populated triplet decays very slowly. Here T_1 acts as a trap state and plays a vital role in triplet exciton migration as revealed by the WG results. Hence, it can be concluded that the peculiar helical molecular packing results in a long phosphorescence lifetime of **3a** compared to other molecules in the series and it is substantiated by the crystal structure and phosphorescence lifetime. In all other cases, the triplet states mostly undergo nonradiative internal conversions compared to radiative transitions.

CONCLUSION

In summary, we have reported a new series of phenylmethanone functionalized N-alkylated carbazoles exhibiting UOP. A helical array by the peculiar molecular packing of 3,6-bis(phenylmethanone) substituted 9-hexylcarbazole in the crystal state enabled to mix up the singlet-triplet states to create hybrid triplets to enhance the intersystem crossings. By optimizing the molecular structure and a strained crystal packing, a metal- and heavy atom-free carbazole derivative resulted in a significant improvement of phosphorescence lifetime and quantum yield. A combined experimental and theoretical study sheds light on the stabilization of the triplet state by the helical arrays and the presence of triplet exciton migration results in the longer phosphorescence lifetime, so far reported for a single molecule crystal. The findings put forth a new strategy of helical arrays to support long-lived phosphorescence under ambient conditions and definitely will invoke the development of new organic phosphors.

Acknowledgements

ADN and Goudappagouda acknowledge University Grants Commission (UGC), India, for fellowship. RK thanks the Department of Higher Education, Government of Kerala for the funding of instrumentation facility in the Government College for Women, Thiruvananthapuram. This work is supported by SERB, Govt. of India, CRG/2019/002539.

Keywords: ultralong phosphorescence • carbazole • waveguiding • phenylmethanone • helicity

[1] a) A. Forni, E. Lucenti, C. Botta, E. Cariati, *J. Mater. Chem. C.* **2018** *6*, 4603; b) M. Baroncini, G. Bergamini, P. Ceroni, *Chem. Commun.* **2017**, *53*, 2081; c) G. Baryshnikov, B. Minaev, H. Ågren, *Chem. Rev.* **2017**, *117*, 6500; d) X. Yang, G. Zhou, W-Y. Wong, *Chem. Soc. Rev.* **2015**, *44*, 8484.

[2] a) Z. Yu, Y. Wu, L. Xiao, J. Chen, Q. Liao, J. Yao, H. Fu, *J. Am. Chem. Soc.* **2017**, *139*, 6376; b) S. M. A. Fateminia, Z. Mao, S. Xu, Z. Yang, Z. Chi, B. Liu, *Angew. Chem. Int. Ed.* **2017**, *56*, 12160; *Angew. Chem.* **2017**, *129*, 12328; c) G. Zhang, G. M. Palmer, M. Dewhirst, C. L. Fraser, *Nat. Mater.* **2009**, *8*, 747.

[3] a) V. C. Wakchaure, K. C. Ranjeesh, Goudappagouda. T. Das, K. Vanka, R. Gonnade, S. S. Babu, *Chem. Commun.* **2018**, *54*, 6028; b) G. He, B. D. Wiltshire, P. Choi, A. Savin, S. Sun, A. Mohammadpour, M. J.

Ferguson, R. McDonald, S. Farsinezhad, A. Brown, K. Shankar, E. Rivard, *Chem. Commun*. **2015**, *51*, 5444.

[4] a) Goudappagouda, A. Manthanath, V. C. Wakchaure, K. C. Ranjeesh, T. Das, K. Vanka, T. Nakanishi, S. S. Babu, *Angew. Chem. Int. Ed.* **2019**, *58*, 2284; *Angew. Chem.* **2019**, *131*, 2306; b) O M. S. Kwon, D. Lee, S. Seo, J. Jung, J. Kim, *Angew. Chem. Int. Ed.* **2014**, *53*, 11177; *Angew. Chem.* **2014**, *126*, 11359; c) Bolten, K. Lee, H. J. Kim, K. Y. Lin, J. Kim, *Nat. Chem*. **2011**, *3*, 205.

[5] a) Kenry, C. Chen, B. Liu, *Nat. Commun.* **2019**, *10*, 2111; b) S. Hirata, *J. Mater. Chem. C.* **2018**, *6*, 11785; c) S. Xu, R. Chen, C. Zheng, W. Huang*, Adv. Mater.* **2016**, *28*, 9920; d) Y. Li, M. Gecevicius, J. Qiu, *Chem. Soc. Rev.* **2016**, *45*, 2090; e) H. Chen, X. Ma, S. Wu, H. Tian, *Angew. Chem. Int. Ed.* **2014**, *53*, 14149; *Angew. Chem.* **2014**, *126*, 14373; f) S. K. Lower, M. A. El-Sayed, *Chem. Rev.* **1966**, *66*, 199.

[6] a) S. Kuila, S. J. George, *Angew. Chem. Int. Ed.* **2020**, 59, DOI:10.1002/anie.202002555; *Angew. Chem. Int. Ed.* **2020**, *132*, DOI:10.1002/ange.202002555; b) S. Kuila, K. V. Rao, S. Garain, P. K. Samanta, S. Das, S. K. Pati, M. Eswaramoorthy, S. J. George, *Angew. Chem. Int. Ed.* **2018**, *57*, 17115; *Angew. Chem.* **2018**, *130,* 17361.

[7] a) R. Kabe, N. Notsuka, K. Yoshida, C. Adachi, *Adv. Mater.* **2016**, *28*, 655; b) S. Hirata, K. Totani, J. Zhang, T. Yamashita, H. Kaji, S. R. Marder, T. Watanabe, C. Adachi*, Adv. Opt. Mater.* **2013**, *1*, 438; c) C. S. Bilen, N. Harrison, D. J. Morantz, *Nature*, **1978**, *271*, 235.

[8] a) Y. Xiong, Z. Zhao, W. Zhao, H. Ma, Q. Peng, Z. He, X. Zhang, Y. Chen, X. He, J. W. Y. Lam, B. Z. Tang, *Angew. Chem. Int. Ed.* **2018**, *57*, 7997; *Angew. Chem.* **2018**, *130*, 8129; b) Z. He, W. Zhao, J. W. Y. Lam, Q. Peng, H. Ma, G. Liang, I. Shuai, B. Z. Tang*, Nat. Commun.* **2017**, *8*, 416; c) W. Zhao, Z. He, J. W. Y. Lam, Q. Peng, H. Ma, Z. Shuai, G. Bai, J. Hao, B. Z. Tang, *Chem.* **2016**, *1*, 592.

[9] a) L. Gu, H. Shi, M. Gu, K. Ling, H. Ma, S. Cai, L. Song, C. Ma, H. Li, G. Xing, X. Hang, J. Li, Y. Gao, W. Tao, Z. Shuai, Z. An, X. Liu, W. Huang, *Angew. Chem. Int. Ed.* **2018**, *57*, 8425; *Angew. Chem.* **2018**, *130*, 8561; b) S. Cai, H. Shi, Z. Zhang, X. Wang, H. Ma, N. Gan, Q. Wu, Z. Cheng, K. Ling, M. Gu, C. Ma, L. Gu, Z. An, W. Huang, *Angew. Chem. Int. Ed.* **2018**, *57*, 4005; *Angew. Chem.* **2018**, *130*, 4069; c) Z. An, C. Zheng, Y. Tao, R. Chen, H. Shi, T. Chen, Z. Wang, H. Li, R. Deng, X. Liu, W. Huang, *Nat. Mater.* **2015**, *14*, 685.

[10] a) Z. He, H. Gao, S. Zhang, S. Zheng, Y. Wang, Z. Zhao, D. Ding, B. Yang, Y. Zhang, W. Z. Yuan, *Adv. Mater.* **2019**, *31*, 1807222; b) T. Ogoshi, H. Tsuchida, T. Kakuta, T. Yamagishi, A. Taema, T. Ono, M. Sugimoto, M. Mizuno, *Adv. Funct. Mater.* **2018**, *28*, 1707369; c) S. Hirata, M. Vacha, *Adv. Optical Mater.* **2017**, *5*, 1600996; d) Y. Xie, Y. Ge, Q. Peng, C. Li, Q. Li, Z. Li*, Adv. Mater.* **2017**, *29*, 1606829; e) Z. Yang, Z. Mao, X. Zhang, D. Ou, Y. Mu, Y. Zhang, C. Zhao, S. Liu, Z. Chi, J. Xu, Y.-C. Wu, P.-Y. Lu, A. Lien, M. R. Bryce, *Angew. Chem. Int. Ed.* **2016**, *55*, 2181; *Angew. Chem.* **2016**, *128*, 2221; f) J. Wei, B. Liang, R. Duan, Z. Cheng, C. Li, T. Zhou, Y. Yi, Y. Wang, *Angew. Chem. Int. Ed.* **2016**, *55*, 15589; *Angew. Chem.* **2016**, *128*, 15818; g) Y. Katsurada, S. Hirata, K. Totani, M. Watanabe, M. Vacha, *Adv. Optical Mater.* **2015**, *3*, 1726.

[11] a) M. Li, K. Ling, H. Shi, N. Gan, L. Song, S. Cai, Z. Cheng, L. Gu, X. Wang, C. Ma, M. Gu, Q. Wu, L. Bian, M. Liu, Z. An, H. Ma, W. Huang, *Adv. Optical Mater.* **2019**, 1800820; b) B. Zhou, D. Yan, *Adv. Funct. Mater.* **2019**, *29*, 1807599; c) L. Gu, H. Shi, L. Bian, M. Gu, K. Ling, X. Wang, H. Ma, S. Cai, W. Ning, L. Fu, H. Wang, S. Wang, Y. Gao, W. Yao, F. Huo, Y. Tao, Z. An, X. Liu, W. Huang, *Nat. Photonics* **2019**, *13*, 406; d) L. Bian, H. Shi, X. Wang, K. Ling, H. Ma, M. Li, Z. Cheng, C. Ma, S. Cai, Q. Wu, N. Gan, X. Xu, Z. An, W. Huang, *J. Am. Chem. Soc.* **2018**, *140*, 10734; e) Z. Chai, C. Wang, J. Wang, F. Liu, Y. Xie, Y.-Z. Zhang, J.-R. Li, Q. Lia, Z. Li, *Chem. Sci.* **2017**, *8*, 8336.

[12] H. Uoyama, K. Goushi, K. Shizu, H. Nomura, C. Adachi, *Nature* **2012**, *492*, 234.

[13] a) E. Yashima, N. Ousaka, D. Taura, K. Shimomura, T. Ikai, K. Maeda, *Chem. Rev.* **2016**, *116*, 13752; b) C. C. Lee, C. Grenier, E. W. Meijer, A. P. H. J. Schenning, *Chem. Soc. Rev.* **2009**, *38*, 671; c) A Maity, M Gangopadhyay, A Basu, S Aute, SS Babu, A Das, *J. Am. Chem. Soc.* **2016**, *138*, 11113.

[14] a) W. Li, Q. Huang, Z. Mao, Q. Li, L. Jiang, Z. Xie, R. Xu, Z. Yang, J. Zhao, T. Yu, Y. Zhang, M. P. Aldred, Z. Chi, *Angew. Chem. Int. Ed.* **2018**, *57*, 12727; *Angew. Chem.* **2018**, *130*, 12909; b) Z. Zhang, L. Tang, X. Fan, Y. Wang, K. Zhang, Q. Sun, H. Zhang, S. Xue, W. Yang, *J. Mater. Chem. C.* **2018**, *6*, 8984.

[15] N. J. Turro, Modern Molecular Photochemistry, University Science Books, Sausalito, **1978**.

[16] C. Chen, Z. Chi, K. C. Chong, A. S. Batsanov, Z. Yang, Z. Mao, Z. Yang, B. Liu, *ChemRxiv.* **2019**, DOI:10.26434/chemrxiv.9895724.

[17] a) G. Wang, B. Xiong, C. Zhou, Y. Liu, W. Xu, C.-A. Yang, K.-W. Tang, W.-Y. Wong, *Chem. Asian J.* **2019**, *14*, 4365; b) H.-R. Bjørsvik, V. Elumalai, *Eur. J. Org. Chem.* **2016**, 5474.

[18] a) K. Nagarajan, A. R. Mallia, K. Muraleedharan, M. Hariharan, *Chem. Sci.* **2017**, *8*, 1776; b) S. Hirata, M. Vacha, *J. Phys. Chem. Lett.* **2016**, *7*, 1539; c) P. Ravat, T. Šolomek, M. Rickhaus, D. Häussinger, M. Neuburger, M. Baumgarten, M. Juríček, *Angew. Chem. Int. Ed.* **2016**, *55*, 1183; *Angew. Chem.* **2016**, *128*, 1198; d) M. Rickhaus, M. Mayor, M. Juríček, *Chem. Soc. Rev.* **2016**, *45*, 1542.

[19] H. Liu, Z. Bian, Q. Cheng, L. Lan, Y. Wang, H. Zhang, *Chem. Sci.* **2019**, *10*, 227.

[20] A. B. Vasista, H. Jog, T. Heilpern, M. E. Sykes, S. Tiwari, D. K. Sharma, S. K. Chaubey, G. P. Wiederrecht, S. K. Gray, G. V. P. Kumar, *Nano Lett.* **2018**, *18*, 650.

[21] D. Chaudhuri, D. Li, Y. Che, E. Shafran, J. M. Gerton, L. Zang, J. M. Lupton, *Nano Lett.* **2011**, *11*, 488-492.

[22] A. Köhler, H. Bässler, *J. Mater. Chem.* **2011**, *21*, 4003.

10.1002/anie.202005105

Table of Contents

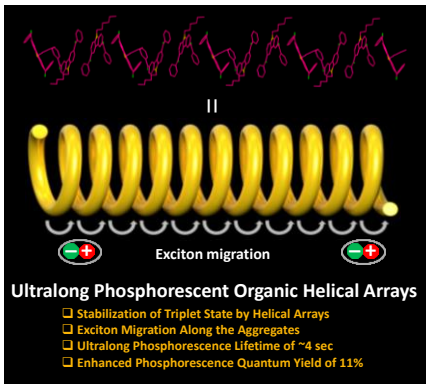

A helical array of phenylmethanone functionalized carbazole with ultralong phosphorescence.